Journal of Statistical Physics, Vol. 70, Nos. 1/2, 1992

Chaotic States in a Random World: Relationship between the Nonlinear Differential Equations of Excitability and the Stochastic Properties of Ion Channels

Louis J. DeFelice[1] and Aurora Isaac[1]

Excitable membranes allow cells to generate and propagate electrical signals. In the nervous system these signals transmit information, in muscle they trigger contraction, and in heart they regulate spontaneous beating. A central question in excitability theory concerns the relationship between the aggregate properties of membranes (marcoscopic) and the properties of channels in the membranes (mircoscopic). Hodgkin and Huxley (1952) laid the foundations of membrane excitability, and Neher and Sakmann (1976) developed techniques to study individual channels. This article focuses on the relationship between the macroscopic domain, in which non-linear differential equations determine the electrical properties of cells, and the microscopic domain, in which the probabilistic nature of channels establishes the pattern of activity. Using nerve cell membranes as an example, we examine how information in one domain predicts behavior in the other. We conclude that the probabilistic nature of channels generates virtually all macroscopic electrical properties, including resting potentials, action potentials, spontaneous firing, and chaos.

KEY WORDS: probabilistic ion channels; resting potential; action potential; spontaneous firing; chaos.

1. INTRODUCTION

Hodgkin and Huxley represented the excitable membrane in nerve as a set of continuous, parallel pathways for the passage of ionic and capacitive

[1] Anatomy and Cell Biology, Emory University School of Medicine, Atlanta, Georgia 30322.

822/70/1-2-22

currents. According to this view, the transmembrane voltage V obeys the equation

$$\frac{dV}{dt} = -\frac{1}{C}\left[g_{Na}(V-E_{Na}) + g_K(V-E_K) + g_L(V-E_L)\right] \tag{1}$$

In the squid axon, the membrane capacitance C equals $1\ \mu F/cm^2$, the reversal potentials for the Na and K pathways are $E_{Na} = 55$ mV and $E_K = -72$ mV, and the reversal potential for the nonspecific leak pathway is $E_L = -50$ mV. The net current through these separate conductances is zero at -60 mV, the resting potential of the nerve. Na and K conductances are controlled by continuous variables (m and h for Na and n for K) that range between 0 and 1 and obey first-order differential equations with voltage-dependent rate constants (α_m, β_m, α_h, β_h, α_n, β_n). The K conductance is equal to the maximum conductance $\bar{g}_K$ times n^4; the Na conductance equals the maximum conductance $\bar{g}_{Na}$ times m^3h, and the maximum conductance equals the total number of channels times the open channel conductance. All α's and β's depend on V. Thus

$$g_K = \bar{g}_K n^4, \qquad \frac{dn}{dt} = \alpha_n(1-n) - \beta_n n \tag{2}$$

$$\bar{g}_K = \gamma_K N_K,$$

$$g_{Na} = \bar{g}_{Na} m^3 h, \qquad \frac{dm}{dt} = \alpha_m(1-m) - \beta_m m \tag{3}$$

$$\bar{g}_{Na} = \gamma_{Na} N_{Na}, \qquad \frac{dh}{dt} = \alpha_h(1-h) - \beta_h h$$

This set of coupled equations is referred to as the Hodgkin and Huxley equations. We use the term "HH model" to mean any set of equations that have this general structure, though the parameters, the powers of the variables, and the kinds of currents that are present may differ. Such solutions of these equations describe macroscopic excitability, i.e., membranes that generate and propagate action potentials.

Ehrenstein *et al.*[16] bridged the gap between macroscopic and microscopic excitability. They showed that the graded conductance in excitable membranes results from the voltage dependence of random openings of ion channels. Conti *et al.*[7] were able to infer the densities and conductances of individual Na and K channels from noise measurements in nerve axons. Their analysis assumed probabilistic channel kinetics based on an interpretation of the HH equations by Hill and Chen[22] and Stevens.[36] Using the patch-clamp technique, researchers were able to isolate single Na and K channels and directly measure their microscopic behavior.[8,28,35] The

relationship of Na and K channels to membrane noise and to macroscopic and microscopic excitability is developed in detail by DeFelice,[10] Clay and DeFelice,[4] DeFelice and Clay,[12] and Hille.[23]

From this sequence of investigation, the following picture emerged. Ion channels fluctuate among many conformational states. The origin of this fluctuation is thermal motion. Patch-clamp recordings show discrete currents of random duration separated by random intervals. Channels, therefore, are functionally bistable; they are either open, allowing specific ions to cross the membrane, or they are closed. Usually, there is only one open state, but often there is more than one closed state. The transitions are assumed to conform to a Markov process: each channel fluctuates between discrete states, and the transition probabilities depend on the momentary status of the channel, not on its history. Rate constants vary with voltage. Open-state and closed-state histograms of channel activity at a constant voltage are monotonically decreasing functions of time. They indicate the number of conformational states that are open or closed, but the mechanism of voltage sensitivity is unknown. The Na and K channels conform to the following kinetic schemes. For the K channel, $[n4]$ represents the open state. For the Na channel, $m3h1$ represents the open state,[19,1]

$$[n0] \underset{\beta_n}{\overset{4\alpha_n}{\rightleftharpoons}} [n1] \underset{2\beta_n}{\overset{3\alpha_n}{\rightleftharpoons}} [n2] \underset{3\beta_n}{\overset{2\alpha_n}{\rightleftharpoons}} [n3] \underset{4\beta_n}{\overset{\alpha_n}{\rightleftharpoons}} [n4] \tag{4}$$

$$\begin{array}{ccccccc} [m0h1] & \underset{\beta_m}{\overset{3\alpha_m}{\rightleftharpoons}} & [m1h1] & \underset{2\beta_m}{\overset{2\alpha_m}{\rightleftharpoons}} & [m2h1] & \underset{3\beta_m}{\overset{\alpha_m}{\rightleftharpoons}} & [m3h1] \\ \alpha_h \Big\downarrow \Big\uparrow \beta_h & & \alpha_h \Big\downarrow \Big\uparrow \beta_h & & \alpha_h \Big\downarrow \Big\uparrow \beta_h & & \alpha_h \Big\downarrow \Big\uparrow \beta_h \\ [m0h0] & \underset{\beta_m}{\overset{3\alpha_m}{\rightleftharpoons}} & [m1h0] & \underset{2\beta_m}{\overset{2\alpha_m}{\rightleftharpoons}} & [m2h0] & \underset{3\beta_m}{\overset{\alpha_m}{\rightleftharpoons}} & [m3h0] \end{array} \tag{5}$$

The probabilistic interpretation of HH models, which we refer to as CH models, is a composite view based on many authors. Many reviews appeared during the initial years. These give a complete picture of the development of the subject.[5,6,9,10,17,18,31–33,38]

2. METHODS

Membrane voltage traces shown in this paper were generated by the Macrochan 10.4 (MCHAN) computer program.[13] This program calculates V in two ways. It uses the HH class of models, which are differential equation models based on whole-cell properties. It also uses CH models, which simulate the random opening and closing of individual channels

under conditions of changing voltage. Each type of model, HH and CH, simulates channels with specified states and experimentally determined, voltage-dependent rate constants. In the HH models, each set of each type of channel shifts continuously and monotonically from state to state. In the CH model, each individual channel walks randomly among the accessible states, and voltage-dependent rate constants determine the probabilities.

To get from $V(t)$ to $V(t+\Delta t)$ with HH models, the voltage-dependent rate constants are determined, and the currents are evaluated from the equations

$$I_K = g_K(V - E_K) \tag{6}$$

$$I_{Na} = g_{Na}(V - E_{Na}) \tag{7}$$

These currents are then used to determine $V(t+\Delta t)$ with the equation

$$V(t+\Delta t) = V(t) - (I_{stim} + I_{Na} + I_K)\,\Delta t/C \tag{8}$$

To get from $V(t)$ to $V(t+\Delta t)$ with the CH model, the probabilities p_{ij} that each channel will change from its present state i to any accessible state j (including its present state) are determined from the voltage-dependent rate constants and arrayed contiguously along the line segment from 0 to 1. The value of a random number between 0 and 1 falls within the range of one p_{ij} along this line segment, thus selecting state j for the next time interval. $V(t+\Delta t)$ is determined by summing the resulting currents for each channel type and evaluating Eq. (8). In repeated runs, from a given $V(t)$, the HH models will always produce the same value for $V(t+\Delta t)$, but the CH model produces different values for $V(t+\Delta t)$ that vary randomly.

Two channel types, Na and K, were used to generate the figures in this paper. The individual channel properties, specified in Table I, were not varied. In the HH models, single-channel conductance and total channel number are related to the membrane conductance through Eqs. (2) and (3). The membrane capacitance of 1 μF/cm^2 was held constant. No leak current was used in these simulations. Parameters that varied were (a) the absolute number of each channel type and (b) the size of the membrane. Changing these parameters allowed variation in the density of channels and the ratio of Na to K channels. The absolute number of channels of each type was altered by varying N_K and N_{Na} in Eqs. (2) and (3). The membrane area was altered by varying C in Eq. (8) in both models. V was calculated at 5-μsec intervals and plotted at 0.2-msec intervals. Except for the initialization demonstrated in Fig. 3, all figures were generated in free-run mode and were offset from the beginning of the run to eliminate transients.

The interbeat intervals (IBIs) were calculated from MCHAN output with a program used to determine the time interval between an arbitrarily

Table I. Ion Channel Parameters[a]

Na	K
$E_{Na} = 55$ mV	$E_K = -72$ mV
$\gamma_{Na} = 6$ ps	$\gamma_K = 4$ ps
$\alpha_m = \frac{-0.1(V+35)}{e^{-(V+35)/10}-1}$	$\alpha_n = \frac{-0.01(V+50)}{e^{-(V+50)/10}-1}$
$\beta_m = 4e^{-(V+60)/18}$	$\beta_n = 0.125e^{-(V+60)/80}$
$\alpha_h = 0.07e^{-(V+60)/20}$	
$\beta_h = \frac{1}{e^{-(V+30)/10}+1}$	

[a] The rate constants are in units of msec^{-1}, and V is in mV.

selected, identifiable feature of each successive pulse. The point at which the increasing voltage crossed -20 mV was chosen because all oscillating traces crossed this voltage with a sharp upward slope. In the IBI plots, the first 5 intervals were excluded to eliminate transients. From runs of 500 msec, IBI plots typically included 40–60 intervals. The IBI plots are return maps, where each point represents a pulse interval i plotted on the x axis against the interval $i+1$ plotted on the y axis.

MCHAN was written by Bill Goolsby and Lou DeFelice for IBM-compatible machines running DOS 3.0 or later with 640K RAM, a match coprocessor, and Hercules CGA, VGA, EGA, or compatible color graphics. MCHAN outputs an ASCII format that can be imported into other programs for further processing. MCHAN is available on request.

3. RESULTS

The relative number of each type of channel in the membrane determines the resting potential of an unstimulated membrane. In Fig. 1, as the absolute number of channels and their density is varied, the ratio of channels is held at Na:K::10:1. The HH model, in this particular simulation, produces a rest potential of -32.2 mV in each case. This is a constant in the HH model, but an average for the CH model. For small numbers of channels, as in Fig. 1a, the variation in V is much greater than that for larger numbers of channels, as in Figs. 1b and 1c. An increase in

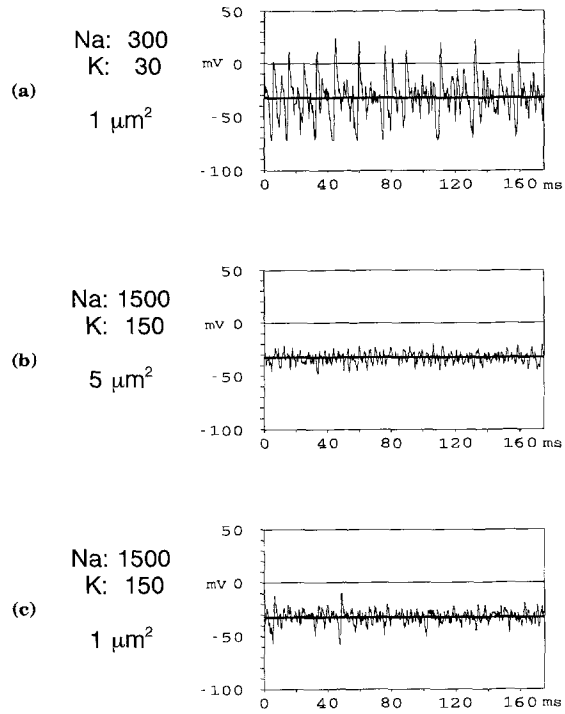

Fig. 1. The difference in noise due to varying absolute and relative numbers of channels. These traces were generated in free-run mode with no stimulus current. The thin line represents V generated by the CH model, and the heavy dark line represents V generated by the HH model. In each trace, $t = 0$ is offset 25 msec from the beginning of the run to eliminate transients. All traces were generated for a Na:K channel ratio of 10:1. N_{Na}, N_K, and C were varied such that (a) was generated for 300 Na and 30 K channels in 1 μm^2 of membrane area, (b) was generated for five times the absolute number of channels as (a) in 5 times the membrane area, thus maintaining the same density of channels, and (c) was generated for the same membrane area as (a), but 5 times the density of channels.

membrane area, modeled by an increase in capacitance, smooths the trace and decreases the variance, as seen in Figs. 1b and 1c.

Perturbation of the steady-state dynamics by an applied current stimulus produces unpredictable variations in the CH model. Figure 2a shows the constant, steady-state V with no stimulus applied. In response to an applied sinusoidal stimulus of the form $B\sin(2\pi ft)$, the HH model oscillates in a repetitious, nonsinusoidal pattern at the same frequency f, as shown in Fig. 2b. If the perturbation is large enough, the voltage contains nonlinear components.[11] The CH model shows this same oscillation with its accompanying noise, but also produces some irregular spikes. If

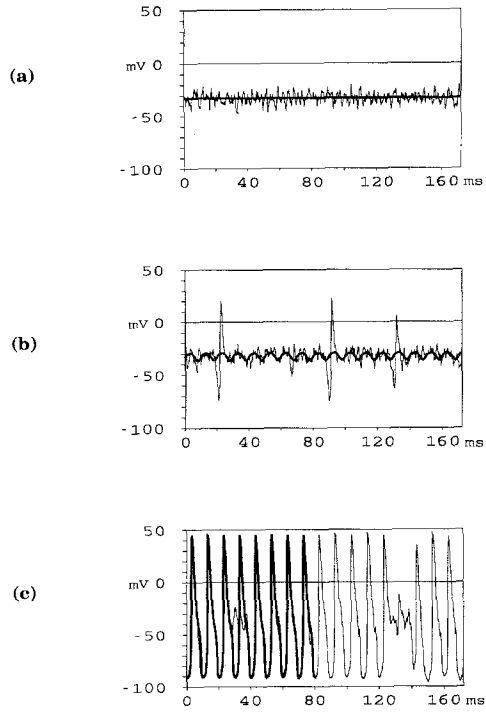

Fig. 2. The effect of applying a current stimulus to the membrane. All traces were generated for 1500 Na channels and 150 K channels in 5 μm^2 of membrane area. In each trace, the light lines represent V generated by the CH model, while the heavy dark lines represent V generated by the HH model. In (c) the HH model was only plotted for $t=0$ to $t=80$ so the CH trace can be visualized. In each trace $t=0$ is offset from the beginning of the run to eliminate transients. (a) Generated with no stimulus current, identical to Fig. 1b. (b) Generated with an applied stimulus of $[3\sin(2\pi \times 100\ \text{Hz} \times t)]$ pA. (c) Generated with an applied stimulus of $[-4+3\sin(2\pi \times 100\ \text{Hz} \times t)]$ pA. The fundamental output V frequency in (b) and (c) is the same as the applied stimulus frequency.

constant current is applied to the membrane such that the steady-state V is sufficiently hyperpolarized, the membrane beats spontaneously. In Fig. 2c, the applied stimulus is of the form $A+B\sin(2\pi ft)$. In this case, A was insufficient to induce spontaneous beating, but the added amplitude B of the sinusoid induced a beat pattern. Although the HH model is extremely consistent from pulse to pulse, the CH model shows irregularities, including an occasional skipped beat.

Reducing the ratio of Na to K channels converts a quiescent membrane into a beating membrane. This is demonstrated in Fig. 3. To portray explicitly the dependence of short-term, transient and long-term, steady-state dynamic patterns on initial conditions, these runs were voltage

clamped at $V=0$ for 10 msec, then allowed to free run at $t=0$. All other data were produced in free-run mode with V initialized to 0. Since we are primarily interested in steady-state dynamics, and not in the transient dynamics of initialization, all other figures were generated with an offset to eliminate transients. The arrow in Fig. 3a shows the minimum offset. For the channel ratio Na:K::10:1, the initialization transients damp quickly. Upon increasing the number of K channels to achieve a Na:K ratio of 5:1, as shown in Fig. 3b, the membrane approaches spontaneous oscillation. The HH model damps slowly to a constant V, but the CH model shows large, irregular, recurrent oscillations. As the ratio Na:K is further decreased to 3:1, as in Fig. 3c, the membrane beats spontaneously and

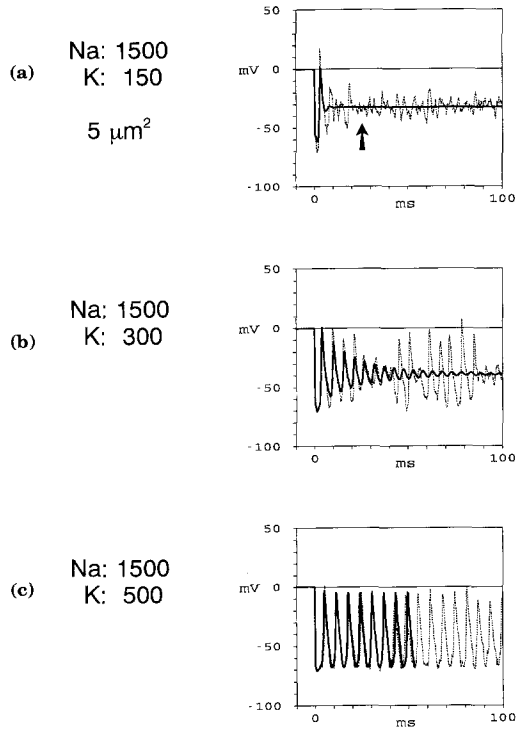

Fig. 3. The effects of initialized variables and parameters on the dynamics of V. Each trace was generated by voltage clamping at 0 mV for 10 msec, then shifting to free run. Unlike the other figures in the paper, these traces are shown from the beginning of each run. The arrow in (a) shows a typical minimum offset for the other figures. No stimulus current was applied in any trace. The light dotted lines represent V generated by the CH model, while the heavy dark lines represent V generated by the HH model. In (c), the repetitious HH trace was partially plotted so the CH trace can be visualized. All traces were generated for 1500 Na channels in 5 μm^2 of membrane area. (a) Channel ratio of Na:K is 10:1, (b) ratio 5:1, (c) ratio 3:1.

regularly. The voltage amplitudes generated by the two models are approximately the same. The voltage irregularities in the CH model reduce the average frequency, causing the two traces to shift in and out of phase.

Applying oscillating current stimuli of varying frequencies to a beating membrane produces varying dynamic states with the HH model that seem to disappear with the CH model. If a constant current stimulus is applied, the frequency and amplitude of pulses are both increased. and pulse shape remains constant from beat to beat. When a sinusoidal stimulus of the form $A + B\sin(2\pi ft)$ is applied and f is varied, the resulting V patterns become irregular, and pulse shape is not necessarily constant from beat to beat. Figure 4 shows three typical patterns for the HH model. The time domain plots of V and the IBI return maps both show very regular patterns. With a 40-Hz stimulus, V appears to have a repeating, three-beat pattern. From

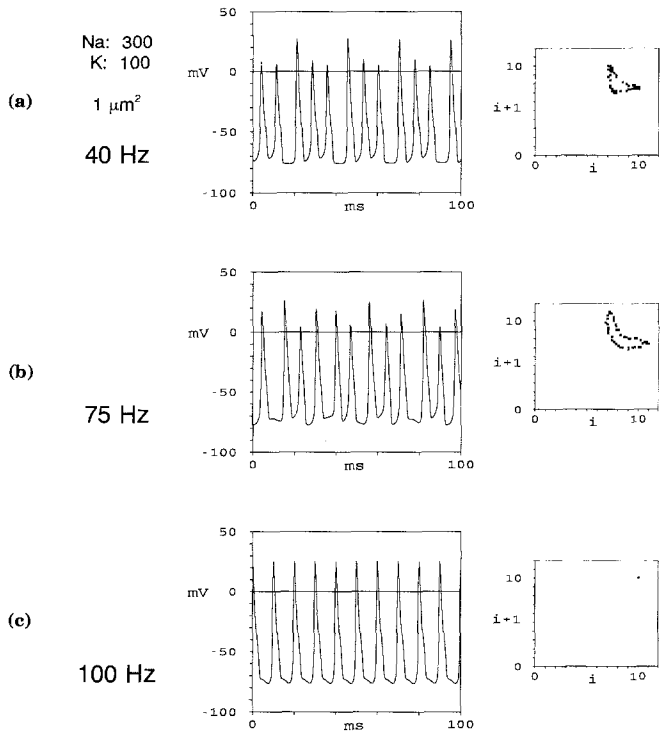

Fig. 4. The effect of varying the applied stimulus frequency. All traces were generated with the HH model at 300 Na and 100 K channels in 1 μm^2 membrane area. The stimulus applied was $[-1 + 0.5\sin(2\pi ft)]$ pA, where (a) $f = 40$ Hz, (b) $f = 75$ Hz, and (c) $f = 100$ Hz. Each set was run for 500 msec. The left traces show a sample of the time domain offset 50 msec from the beginning of the run. The right traces are the IBI return maps plotted in msec. The first 5 intervals were not plotted, to avoid transients.

the IBI plot, this pattern seems to be drifting toward chaos. The 75-Hz pattern is irregular and chaotic, whereas the 100-Hz pattern is repetitious from pulse to pulse. These three solutions are distinct in the HH model. Figure 5 shows three typical patterns for the CH model, generated under conditions analogous to those of Fig. 4. The three IBI plots in Fig. 5 do not reveal any distinguishing characteristics.

As the number of channels is increased, the CH model begins to show the deterministic patterns of the HH models. Figure 6a shows the HH and CH models superimposed for a stimulus frequency of 60 Hz. At this frequency, the HH model shows a repetitious two-pulse pattern resulting in two distinct points on the IBI return map. The CH model shows irregularities, with some suggestion of the two-beat pattern in the V time

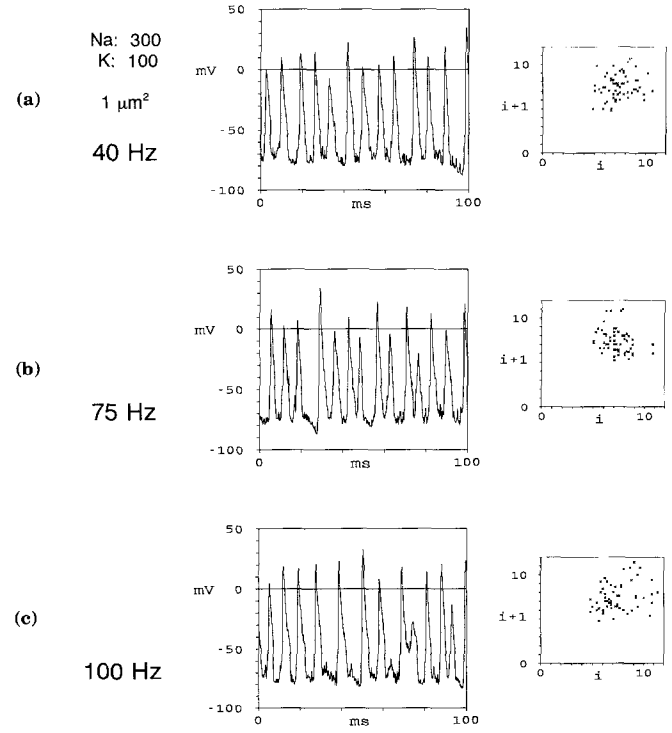

Fig. 5. The effect of varying the applied stimulus frequency. This figure is identical to Fig. 4 in all respects except that it was generated with the CH model instead of the HH model. All traces were generated with 300 Na and 100 K channels in 1 μm^2 membrane area. The stimulus applied was $[-1+0.5\sin(2\pi ft)]$ pA, where (a) $f=40$ Hz, (b) $f=75$ Hz, and (c) $f=100$ Hz. Each set was run for 500 msec. The left traces show a sample of the time domain offset 50 msec from the beginning of the run. The right traces are the IBI return maps plotted in msec. The first 5 intervals were not plotted, to avoid transients.

domain trace, but the IBI plot shows the same random scatter seen in Fig. 5. Increasing the number, but not the density, of channels causes the IBI plot to coalesce into two smaller scatters surrounding the two HH points (Fig. 6b). The same number of channels at higher density (Fig. 6c) results in IBIs like the HH patterns seen in Figs. 4a and 4b.

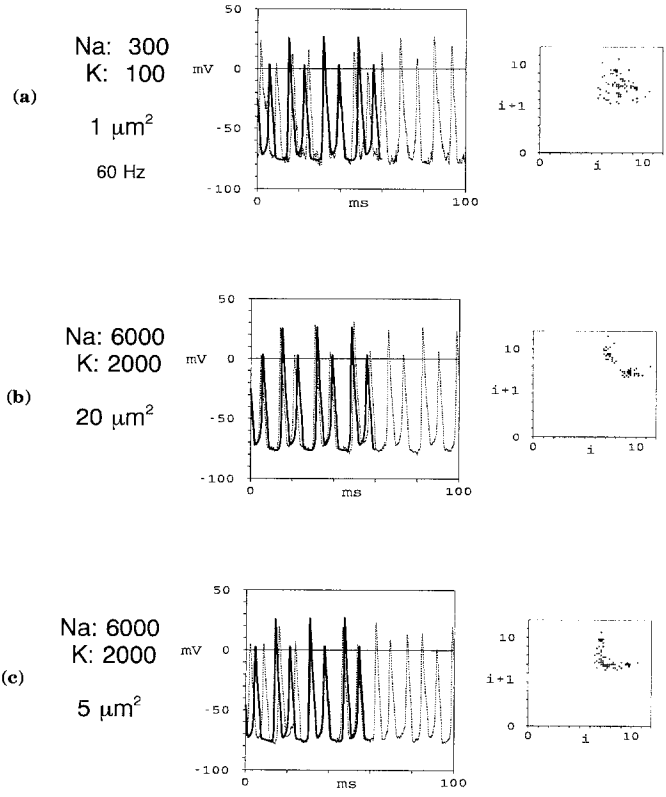

Fig. 6. The convergence of the HH and CH models as the number of channels is increased. The left trace shows a sample of the time domain of V offset from the beginning of the run. The light, dotted line represents the CH model, while the heavy dark line represents the HH model. The repetitious HH model was partially plotted to allow visualization of the CH trace. The HH model is represented in the IBI return plots by dark squares, while the CH model is represented by plus signs. In (a) V was generated for 300 Na and 100 K channels in 1 μm^2 of membrane area. The applied stimulus was $[-1+0.5\sin(2\pi ft)]$ pA with $f=60$ Hz. In (b) the number of channels, membrane area, and stimulus amplitude were all multiplied by 20. In (c) the number of channels and stimulus amplitude were multiplied by 20, but the membrane area only by 5. Thus, the density is preserved from (a) to (b), but increased by a factor of 4 in (c).

4. DISCUSSION

The characteristics of ion channels in the cell membrane determine the electrical properties of nerve, skeletal muscle, cardiac muscle, and virtually all excitable tissues. Channels act as selective pores for specific ions such as Na, K, and Ca. These proteins are embedded in a lipid bilayer that acts as a parallel capacitor. The essential nature of ion channels is stochastic. Thermal motion causes them to gate randomly, and transmembrane voltage biases the gates. The ion gradients that exist across cell membranes amplify the relatively low thermal energy of the gates into an appreciable signal. The net result is a voltage-dependent, time-variant kinetics of ion channels, which, in combination with the membrane capacitance, gives rise to virtually all macroscopic electrical properties. These properties include the cell resting potential, the generation and propagation of action potentials, extracellular field potentials, spontaneous firing, and intercellular communication. Such phenomena come about in the free-running membrane because channels open or close. Other channels sense this voltage and modify their kinetics accordingly. The extent to which channels communicate depends on how close they are to one another. It also depends on the status of the interposed channels, the membrane capacitance, and the intracellular and extracellular resistivities. In this paper, we have dealt only with the restricted problem of the space-clamped membrane, in which the voltage is instantaneous over the channel population.

The interpretation of excitability we have made is consistent with the two main experimental observations obtained from patch-clamp techniques: (a) channels flip randomly between two states, one with zero conductance and the other with constant conductance; (b) the mean intervals between open and closed states are voltage dependent. Under this interpretation, assuming only one closed and one open state, the macroscopic rate constants $\alpha_n(V)$ and $\beta_n(V)$ have the following meaning: if a channel is closed, the probability it will remain closed for a time Δt is $\exp[-\alpha_n(V)\,\Delta t]$; if a channel is open, the probability it will remain open for a time Δt is $\exp[-\beta_n(V)\,\Delta t]$, where Δt is small, and V is constant over Δt. More complex schemes have analogous formulas. This formulation is sufficient to explain the voltage and time dependence of membrane conductance. Channels may have a single gate or a series of identical gates, like the K channel in Eq. (4), or they may have different kinds of gates, like the activating and inactivating gates of the Na channel in Eq. (5). The present simulations correspond to a strict interpretation of HH kinetics in which the gates are independent. Other models are amenable to these same simulation techniques.

The fundamental difference between the HH and CH models is

demonstrated in Fig. 1. The HH model treats all channels of a single type as a single, homogeneous unit modeled by population characteristics. If only K channels were present, V would remain constant at -72 mV. If only Na channels were present, V would remain constant at 55 mV. When both are present, the rest potential represents a balance point between these two extremes that depends on the ratio of Na to K channels. In Fig. 1, as the absolute number or density of channels changes, V remains constant in the HH model as long as the ratio Na:K remains constant. The CH model includes population properties, but it also includes thermal properties of individual channels. Thus, the numbers of open K channels and open Na channels change. This causes the balance point of V to change and produces "noise." For small populations of channels (Fig. 1a) each channel represents a larger fraction of the total than for larger populations (Figs. 1b and 1c). The noise is greater for small populations, but average V is the same for large and small populations. Hence, it is the same for both the HH and CH models.

HH dynamics plus noise do not simply equate to CH dynamics. In Fig. 2, we perturb the constant-voltage dynamics to demonstrate this feature. The irregular spikes generated in the CH dynamics, shown in Fig. 2b, represent a frequency dependent entrainment of the spontaneous fluctuations. These dynamics can lead to significant divergence between the two models, such as the skipped beats in Fig. 2c. Although similar dynamics could result from HH plus noise, the spectral density, the magnitude, and the origin of the added noise have no primary interpretation. In the CH approach, the noise has an inherent physical meaning.

The nonlinear channel properties can produce a variety of dynamic patterns. If we start with only Na channels and add a relatively small number of K channels, the system rests at a constant V as in Fig. 1. If V is hyperpolarized sufficiently, the time-dependent properties of the channels are such that an action potential is triggered. Hyperpolarization results from adding a leak current, applying a hyperpolarizing stimulus current as in Fig. 2c, or adding more K channels as in Fig. 3c. With the HH model, the dynamics shift suddenly, as K is varied, from constant to beating. For parameters in the region in which the HH dynamics changes from constant to beating, the CH model tends to waver between the two. As in Fig. 3b, the CH model may beat irregularly when the HH model is constant. If K were to increase even more, e.g., Na:K::1:2, V would hyperpolarize past the range that allows beating, and V would remain constant, close to E_K.

Many types of cells either beat intrinsically, or they will beat under certain conditions. These cells may interact with other inherent oscillators. Stimulating a beating membrane with a sinusoidal stimulus models this interaction. Differential equations exhibit diverse patterns of oscillation as

we vary the stimulating frequency (Figs. 4 and 6a). With the CH model, as (Fig. 5 and Fig. 6a), distinct states do not appear evident. However, increasing the number of channels causes the CH model to approach the same attractors as appear in the HH model (Fig. 6b and 6c). We call these solutions chaotic, not in the strict sense of positive Liapunov exponents, but rather in the vernacular sense. These attractors arise without benefit of the differential equation.

This result suggests that the chaotic solutions of macroscopic equations are epiphenomena. Macroscopic, nonlinear differential equations actually represent a large population of individual events. HH equations have no predictive value about single-channel kinetics beyond how they will behave on average. The mean open time of an individual channel equates with the macroscopic relaxation of an ensemble of channels; thus, $\beta(V)$ that appears in the CH simulation is the same $\beta(V)$ that appears in the HH equations. The CH model has individual and population behavior, whereas the HH model includes only population information. The HH model is only capable of deterministic solutions; even irregular, chaotic solutions represent the average behavior of large populations.

We began with the random properties of individual channels and obtained the chaotic behavior of populations of channels. We showed similar kinetics from a global model. Are these kinetics inherent to both models, or are cells fundamentally stochastic or chaotic? Both models are an approximation. For example, Na and K channels are coupled by a shared voltage. This is an oversimplification. Not only do other kinds of channels exist, but channels depend on factors besides membrane voltage. For example, Ca channels may be coupled by shared Ca.[15,29] The Markov representation is also an oversimplification. Channel models based on the chaotic properties of intramolecular states have been proposed.[26,27] Noise of the type observed in membranes could be obtained with deterministic models as well as stochastic models. Certainly, interbeat interval fluctuations[3] and other fluctuations in action potential kinetics and action potential amplitudes can derive from deterministic models.[2,20,21,25] The Liebovitch suggestion requires that individual channels obey deterministic equations. We would maintain that, even if the internal gates or external coupling contribute a deterministic component to open-close kinetics, the underlying process remains stochastic. We conclude that bistable, random events generate virtually all macroscopic electrical properties of cells, not only resting potentials, action potentials, spontaneous firing, but also chaos.

ACKNOWLEDGMENTS

We wish to thank W. N. Goolsby for the continued development of the program, MCHAN, that we used for the present simulations. This work was supported by NIH grant 1-PO1-HL27385.

REFERENCES

1. C. M. Armstrong, Inactivation of the potassium conductance and related phenomena caused by quaternary ammonium ion injected in squid axons, *J. Gen. Physiol.* **54**:553–575 (1969).
2. D. R. Chialvo, R. F. Gilmour, Jr., and J. Jalife, Low dimensional chaos in cardiac tissue, *Nature* **343**:653–657 (1990).
3. J. R. Clay and R. L. DeHaan, Fluctuations in interbeat interval in rhythmic heart-cell clusters: Role of membrane voltage noise, *Biophys. J.* **28**:377–390 (1979).
4. J. R. Clay and L. J. DeFelice, Relationship between membrane excitability and single channel open–close kinetics, *Biophys. J.* **42**:151–157 (1983).
5. F. Conti, Noise analysis and single-channel recordings, *Curr. Top. Membrane Trans.* **22**:371–405 (1984).
6. F. Conti and E. Wanke, Channel noise in membranes and lipid bilayers, *Q. Rev. Biophys.* **8**:451–506 (1975).
7. F. Conti, L. J. DeFelice, and E. Wanke, Postassium and sodium ion current noise in the membrane of the squid giant axon, *J. Physiol.* (London) **248**:45–82 (1975).
8. F. Conti and E. Neher, Single channel recordings of K currents in squid axon, *Nature* **285**:140–143 (1980).
9. L. J. DeFelice, Fluctuation analysis in neurobiology, *Int. Rev. Neurobiol.* **20**:169–208 (1977).
10. L. J. DeFelice, *Introduction to Membrane Noise* (Plenum Press, New York, 1981).
11. L. J. DeFelice, W. J. Adelman, Jr., D. E. Clapham, and A. Mauro, Second-order admittance in squid axon, in *The Biophysical Approach to Excitable Systems*, W. J. Adelman, Jr. and D. E. Goldman, eds. (Plenum Press, New York, 1981).
12. L. J. DeFelice and J. Clay, Membrane channel and membrane potential from single-current kinetics, in *Single-Channel Recording*, B. Sakmann and E. Neher, eds. (Plenum Press, New York, 1983).
13. L. J. DeFelice, W. N. Goolsby, and D. Huang, Membrane noise and excitability, in *Noise in Physical Systems*, A. D'Amico and P. Mazzetti, eds. (Elsevier, Amsterdam, 1985).
14. L. J. DeFelice, Noise biological membranes, in *Noise in Physical Systems*, A. Ambrozy, ed. (Elsevier, Amsterdam, 1989).
15. L. J. DeFelice, Molecular biology and biophysics of Ca channels: A hypothesis concerning oligomeric structure, channel clustering, and macroscopic current, in *Neural Engineering*, Y. Kim and X. Thakor, eds. (Springer-Verlag, Heidelberg, 1992).
16. G. Ehrenstein, H. Lecar, and R. Nossal, The nature of the negative resistance in bimolecular lipid membranes containing excitability inducing material, *J. Gen. Physiol.* **55**:119–133 (1970).
17. G. Ehrenstein and H. Lecar, Electrically gated ionic channels in lipid bilayers, *Q. Rev. Biophys.* **10**:1–34 (1977).
18. G. Feher, Emerging techniques: Fluctuation spectroscopy, in *Trends in Biochemical Sciences* (Elsevier, Amsterdam, 1978), Vol. 3, pp. 111–113.
19. R. FitzHugh, A kinetic model of the conductance changes in nerve membrane, *J. Cell Comp. Physiol.* **66**:111–118 (1965).

20. J. R. Guevara, A. C. G. van Ginneken, and H. J. Jongsma, Patterns of activity in a reduced ionic model of a cell from the rabbit sinoatrial node, in *Chaos in Biological Systems*, H. Degn, A. V. Holde, and L. F. Olsen, eds. (Plenum Press, New York, 1987).
21. J. R. Guevara, Mathematical modeling of the electrical activity of cardiac cells, in *Theory of Heart*, L. Glass, P. Hunter, and A. McCullogh, eds. (Springer, New York, 1990).
22. T. L. Hill and Y.-D. Chen, On the theory of ion transport across nerve membrane IV: Noise from the open–close kinetics of K channels, *Biophys. J.* **12**:948–959 (1972).
23. B. Hille, *Ionic Channels of Excitable Membranes* (Sinauer, Sunderland, Massachusetts, 1992).
24. A. L. Hodgkin and A. F. Huxley, A qualitative description of membrane current and its application to conduction in nerve, *J. Physiol.* **177**:440–544 (1952).
25. T. J. Lewis and M. R. Guevara, Chaotic dynamics in an ionic model of the propagated cardiac action potential, *J. Theor. Biol.* **146**:407–432 (1990).
26. L. S. Liebovitch and T. I. Toth, A model of ion channel kinetics using deterministic chaotic rather than stochastic processes, *J. Theor. Biol.* **148**:243–267 (1991).
27. L. S. Liebovitch, Interpretation of protein structure and dynamics from the statistics of the open and closed times measured in a single ion-channel protein, *J. Stat. Phys.* **70**:329–337 (1993).
28. I. Llano, C. K. Webb, and F. Bezanilla, Potassium conductance of the squid giant axon, *J. Gen. Physiol.* **92**:179–196 (1988).
29. M. Mazzanti, L. J. DeFelice, Y. M. Liu, Gating of L-type Ca currents in embryonic chick ventricle cells: Dependence on voltage, current, and channel density, *J. Physiol.* **443**:307–334 (1991).
30. E. Neher and B. Sakmann, Single-channel currents recorded from membrane of denervated frog muscle fibres, *Nature* **260**:779–802 (1976).
31. E. Neher and C. F. Stevens, Conductance fluctuations and ionic pores in membranes, *Annu. Rev. Biophys. Bioeng.* **6**:345–381 (1977).
32. B. Neumcke, $1/f$ noise in membranes, *Biophys. Struct. Mech.* **4**:179–199 (1978).
33. B. Neumcke, Fluctuation of Na and K currents in excitable membranes, *Int. Rev. Neurobiol.* **23**:35–67 (1982).
34. B. Sakmann and E. Neher, *Single-Channel Recording* (Plenum Press, New York, 1984).
35. F. L. Sigworth and E. Neher, Single Na channel currents observed in cultured rat muscle cells, *Nature* **287**:447–449 (1980).
36. C. F. Stevens, Inferences about membrane properties from electrical noise measurements, *Biophys. J.* **12**:1028–1047 (1972).
37. C. F. Stevens, Principles and applications of fluctuation analysis: A non-mathematical introduction, *Fed. Am. Soc. Exp. Biol.* **34**:1364–1370 (1975).
38. A. A. Verveen and L. J. DeFelice, Membrane noise, *Prog. Biophys. Mol. Biol.* **28**:189–265 (1974).